

Annual validation of significant wave heights of ERS-1 synthetic aperture radar wave mode spectra using TOPEX/Poseidon and ERS-1 altimeter data

Eva Bauer

Potsdam Institute for Climate Impact Research, Potsdam, Germany

Patrick Heimbach¹

Max-Planck-Institut für Meteorologie, Hamburg, Germany

Abstract. Significant wave heights retrieved globally during 1994 from low bit rate imagerie spectra of the synthetic aperture radar (SAR) operating in the intermittent wave mode (SWM) onboard the first European Remote Sensing (ERS-1) satellite (H_s^{swm}) are validated using independent, buoy-validated satellite altimeter data from TOPEX/Poseidon (H_s^{top}) and ERS-1 (H_s^{ers}). H_s^{swm} is retrieved using the extended inversion algorithm of the fully nonlinear wave-to-SAR spectral integral transform [Hasselmann *et al.*, 1996]. The statistical comparison shows that globally retrieved H_s^{swm} agree remarkably well with collocated data of both altimeters. Histograms of global H_s^{swm} are well approximated by the universal lognormal distribution function. A small but systematic underestimation of H_s^{swm} with respect to both altimeters by 0.1 m is noticed. This bias is small compared to the uncorrelated root-mean-square (rms) deviation of 0.5 m. The underestimation originates from underestimations of the high sea states dominated by wind sea. The entire range of swell waves of H_s^{swm} , however, corresponds very closely to H_s^{top} . Thus the high accuracy of SWM-retrieved swell wave heights substantiates their suitability for model validation and for operational wave data assimilation. To achieve also reliable estimates of the high sea states, the combined analysis of wave and wind data from both modeling and observation is the most promising approach.

1. Introduction

Since the launch of the first European Remote Sensing (ERS-1) satellite in July 1991, wave height variance spectra of the ocean surface are routinely retrieved from the synthetic aperture radar (SAR) wave mode imagerie spectra. For the first time, two-dimensional wave spectra from all over the world oceans have now been measured for several years. These spectral wave measurements were awaited for a long time for various applications. A major application consists of validating global spectral wave models to ensure that both the physics and the numerics of the models are appropriately represented. An accurate description of the dynamics of surface waves is closely related to under-

standing the exchange processes at the air-sea interface, such as the flux of momentum, latent and sensible heat, gas, and sea-salt aerosols.

Further applications comprise the assimilation of remotely sensed wave spectra into operational wave prediction models. The update of real-time wave predictions through operational assimilation of wave data is required for the same reasons as is the assimilation of weather data, namely, to update the first-guess fields with observations for improving the forecast calculations. While the assimilation of altimeter wave heights has already been demonstrated to increase the wave forecast skill [Lionello *et al.*, 1995; Janssen *et al.*, 1996], the assimilation of wave spectra is expected to further increase the forecast skill. An improvement of wave forecasts is beneficial for ship routing and for nearshore and offshore activities, particularly for extreme weather conditions [e.g., *European Space Agency (ESA)*, 1996]. Furthermore, wave data assimilation schemes help to find potential errors in the modeled wind fields by utilizing the dynamic relationship between wind and waves [Bauer *et al.*, 1996; Janssen *et al.*, 1996; Bauer *et al.*, 1997; Hasselmann *et al.*, 1997]. As a consequence, wind

¹Now at the Department of Earth, Atmospheric and Planetary Sciences, Massachusetts Institute of Technology, Cambridge, Massachusetts.

Copyright 1999 by the American Geophysical Union.

Paper number 1999JC900014.
0148-0227/99/1999JC900014\$09.00

fields corrected by means of wave data assimilation are expected to improve the estimates of the exchange rates at the air-sea interface.

Moreover, long-term wave measurements indicate wave climate changes [Bacon and Carter, 1991; von Storch et al., 1998; Kushnir et al., 1997; Gulev et al., 1998; Bauer et al., 1999]. It is currently being investigated whether the observed changes are attributed to natural fluctuations or whether they may contain a signal of anthropogenic climate change. In this context, global homogeneous spectral wave data, although yet available over a limited period only, represent valuable information supplementing wave data from local measuring devices (e.g., buoys, ships) and simple wave height data from altimeters to study the wave climate and the causes for wave climate changes.

An essential prerequisite for wave data assimilation and wave climate research is, however, a thorough validation of the measured wave data. A first evaluation of a limited set of ocean wave spectra retrieved from ERS-1 SAR wave mode (SWM) data was performed by Brüning et al. [1994]. An extensive statistical intercomparison using a 3-year global set of the ERS-1 SWM spectral retrievals and the third-generation wave model (WAM) spectra was presented by Heimbach et al., [1998]. The quality of the SWM data and the fidelity of the algorithm to retrieve wave spectra from SAR spectra were assessed.

Complementary to the above quality assessment of the SWM-retrieved wave data, a more general validation against independent and reliable wave measurements remains an essential exercise. Measurements of spaceborne altimeters are highly suitable to serve as independent reference data of high absolute accuracy. Altimeters provide measurements of significant wave height, $H_s = 4\sqrt{E_{\text{tot}}}$, where E_{tot} is the integral over the wave height variance spectrum.

In this study, we validate SWM-retrieved wave heights (H_s^{swm}) using H_s data from the TOPEX (H_s^{top}) and the ERS-1 (H_s^{ers}) altimeters. We collocate H_s^{swm} available for the year 1994 to H_s^{ers} and H_s^{top} and compare them statistically. Dependencies on region and season and on the collocation criteria are examined. Furthermore, an attempt is made to study dependencies on wave conditions by comparing H_s with respect to pure wind sea and swell wave heights. This comparison is stimulated by findings that the wave model WAM tends to overestimate wind sea and to underestimate swell wave height relative to H_s^{swm} [Heimbach et al., 1998].

The paper is organized as follows: Section 2 briefly reviews the processing of the three H_s data sets and describes the data collocation. Results of the statistical intercomparison of the collocated H_s data sets are presented in section 3. In section 4 we attempt to isolate sets of pure wind sea and swell wave heights to determine their statistical correspondence. Conclusions are drawn in section 5.

2. Description of H_s Data Sets

2.1. H_s From ERS-1 SAR Wave Mode Imagette Spectra

The ERS-1 SAR wave mode imagette spectra are disseminated in quasi-real time to users as fast delivery product (FDP). This product is obtained from the SAR operating in the intermittent sampling mode (so-called "wave mode") in which 5×10 km snapshot imagettes of the local ocean surface are taken every 200 km along the satellite track. Because of sufficiently reduced power and data storage requirements, the imagette data can be stored on board and are transmitted once per orbit to the ERS ground-receiving stations where they are processed to power spectra on a reduced polar wavenumber grid [ESA, 1993; Heimbach et al., 1998; Hasselmann et al., 1998].

The SAR is a side-looking active microwave instrument which emits short radar pulses and processes a two-dimensional image from the received radar backscatter. Each image pixel represents the backscatter intensity of 5.3 GHz (C-band) radar pulses in VV polarization emitted at 19.9° incidence angle (during the period of interest). The received intensity is proportional to the energy of the short ripple waves which fulfill the Bragg resonance condition. The SAR image is achieved by measuring the travel time (range) and the Doppler history with respect to the platform velocity (azimuth) of the backscattered radar pulses.

The long ocean waves modulate the short ripple waves which leads to a modulation of the received intensity. The modulation is induced by the long wave's slope and by the hydrodynamic interactions between the short and the long waves which are described by the linear tilt and the hydrodynamic modulation transfer functions. This description applies for the imaging process of frozen surfaces by a real aperture radar (RAR). The SAR imaging of waves is, furthermore, strongly affected by the so-called velocity bunching mechanism, induced by the orbital velocities of the waves. These surface movements cause Doppler frequency shifts in the phase history of the radar backscatter which lead to an effective nonlinear redistribution of the backscattering facets in the SAR image plane (see Alpers and Hasselmann [1978], Alpers et al. [1981], and the MARSEN review [Hasselmann et al., 1985]).

The nonlinear velocity bunching is strong for spaceborne SARs of high distance-to-platform velocity ratio (R/V) and increases with increasing wavenumber and root-mean-square (rms) orbital velocity. This leads, among other effects, to image smearing and to a loss of information beyond the azimuthal cutoff wavenumber, corresponding to length scales shorter than typically 100 to 200 m in the satellite flight direction. In addition, SAR imagette spectra suffer from a 180° frozen-image ambiguity. Despite these difficulties, the SAR imaging mechanism of waves is meanwhile well

understood and was verified in a number of field experiments (see the space shuttle imaging radar missions B and C (SIR-B/C) [Alpers *et al.*, 1986; *Monaldo and Lyzenga*, 1986; *Brüning et al.*, 1988], the Labrador Extreme Waves Experiment (LEWEX) [Beal, 1991], the Synthetic Aperture Radar and X-Band Ocean Nonlinearities - Forschungsplattform Nordsee (SAXON-FPN) campaign [Plant and Alpers, 1994], and the Grand Banks ERS-1 SAR Wave Spectra Validation Experiment [Grand Banks, 1994]).

An efficient iterative inversion algorithm of the closed nonlinear integral, describing the mapping of ocean wave spectra into SAR image spectra [Hasselmann and Hasselmann, 1991], was developed to reliably retrieve ocean wave spectra from SAR image spectra within the computational constraints of real-time operational applications [Hasselmann *et al.*, 1996, 1998].

To compensate for the loss of information beyond the azimuthal cutoff and to remove the ambiguity, a first-guess spectrum is used as input for the retrieval. In our case, the collocated first-guess spectra were provided by the operational WAM model [Hasselmann *et al.*, 1988; Günther *et al.*, 1992] from the European Centre for Medium-Range Forecasts (ECMWF). The first-guess spectra are available from a $3^\circ \times 3^\circ$ latitude/longitude model grid until July 1994 and for the rest of the year from a $1.5^\circ \times 1.5^\circ$ grid. The wind forcing is provided by the 6-hour u_{10} wind analysis at 10 m height of the ECMWF atmospheric model. The operational wave prediction comprises the assimilation of H_s from the ERS-1 altimeter by optimal interpolation every six hours. The wave model data are obtained from the model output after each 6-hour model run before the assimilation is performed [Janssen *et al.*, 1996]. The modeling of the waves is performed only for ice-free areas which are inferred from daily maps of the sea surface temperature analyses provided routinely by NCEP (National Centers for Environmental Prediction) to ECMWF since August 1993. Through the collocation procedure, described later, all data may be considered to be from ice-free areas.

The SAR-to-wave retrieval algorithm incorporates an internal calibration which is independent of the SAR instrument calibration and of measurements of the absolute backscattering cross section. The absolute calibration of the ERS-1 SWM spectra is deduced from evaluating the clutter background noise spectrum which is assumed to be white [Alpers and Hasselmann, 1982; Brüning *et al.*, 1994; Hasselmann *et al.*, 1998].

Three years of ERS-1 SWM data between January 1993 and December 1995, comprising 1.2 million spectra, have been analyzed [Heimbach *et al.*, 1998]. About three quarters of the incoming spectra could successfully be retrieved and provided quantitative estimates of the spectral wave energy. A retrieval is considered successful if the cost function measuring the distance between the SAR image spectrum and the image spec-

trum calculated from the retrieved ocean wave spectrum is less than a typical error bound. This eliminates, in particular, retrievals of SWM with low signal-to-noise ratios. Here the integral values, i.e., H_s of the retrieved wave spectra, of the year 1994 are used for the inter-comparison.

2.2. H_s of TOPEX and ERS-1 Altimeter Data

The significant wave heights obtained from the Ku band TOPEX altimeter of the TOPEX/Poseidon satellite are provided as an off-line product by AVISO (Toulouse, France). The ERS-1 altimeter data used are the fast delivery (FD) product provided by ECMWF (Reading, England).

Satellite altimeters are nadir-looking radars which measure the microwave pulses from specular reflection at the sea surface. A rough, wavy sea surface causes a broadening of the reflected signal; thus from the shape of the averaged returned signal H_s can directly be deduced. The available H_s data from the ERS-1 and the TOPEX altimeter represent averages over 1 s intervals. One 1 s estimate represents an average over a surface area which is determined by the diameter of the footprint of a pulse and by the distance overflown by the satellite within 1 s. The diameter of the footprint is a few kilometers. It increases with increasing wave height to about 10 km for $H_s \approx 10$ m; the flight velocity of the TOPEX and the ERS-1 satellites is about 6 and 7 km/s, respectively.

In the process of quality control a small fraction of the 1s H_s estimates of both satellites were rejected because they were flagged as being either over land or were accompanied with exceptional large rms values of the 1-s average. The FD H_s of ERS-1 required an additional quality control and a correction. Comparisons of FD ERS-1 H_s data against buoy measurements and against TOPEX H_s data revealed a significant underestimation of FD ERS-1 H_s (after the change of the ERS-1 altimeter sensor algorithm in January 1994) [Cotton and Carter, 1994; Queffeuilou, 1996; Bauer and Staabs, 1998]. Linear correction formulas for the FD ERS-1 H_s were determined by P.D. Cotton (personal communication, 1997) and Queffeuilou [1996]. A nonlinear correction was proposed by H. Tolman (personal communication, 1997) to account better for some shortcomings in FD ERS-1 H_s below 1.5 m. The effect of the three different correction formulas appeared nondiscernible for the present analysis. We corrected the FD ERS-1 H_s according to

$$H_s^{\text{ers}} = 1.11H_s^{\text{FD ERS-1}} + 0.09 \quad (1)$$

which was derived using the TOPEX measurements ranging between 1 and 10 m [Queffeuilou, 1996].

The additional quality control applied to H_s of the ERS-1 altimeter eliminated spurious data occurring in coastal regions and for very low sea states. Low sea states cause difficulties to determine a smooth average

pulse form and may lead to large errors in H_s . The spurious data are identified by large fluctuations of neighboring estimates. If the rms fluctuation of three consecutive values lies outside the 99% confidence interval of the three-point mean then the data are rejected. This empirically determined threshold eliminates less than 1% of the data but improved the statistical intercomparison results drastically.

TOPEX-derived H_s were found to be highly reliable, their absolute accuracy being larger than the specified performance goal of 0.5 m or 10%, whichever is larger [Callahan *et al.*, 1994; Cotton and Carter 1994; Gower, 1996]. Collocated H_s^{top} and buoy H_s within the range 0.1 to 8 m (including one case above 12 m), with a temporal separation of less than 37 min and a spatial separation of often less than 40 km show a close correspondence. The H_s^{top} are slightly (about 5%) lower than buoy H_s , with an rms scatter about the mean of 0.3 m [Gower, 1996]. For the following intercomparison we used three-point averages of the altimeter H_s . The averaging over three consecutive 1-s H_s estimates slightly reduces the random variability inherent in the altimeter data.

2.3. Collocation

The H_s data retrieved either from SWM or from altimeter represent an instantaneous measurement averaged over an area of about the same size. The area of the H_s^{swm} data is invariably 5×10 km large; the 3 s average of altimeter H_s represents an area average of about 18×3 km to 21×10 km, varying mainly with satellite flight velocity and wave height. The collocation criteria are defined by the spatial and the temporal distances between the measurements. The distances should be smaller than the typical decorrelation time and length scales to ensure that both measurements are taken from the same geophysical environment. At the same time, the space and time separations should be large enough to obtain a sufficiently large number of collocation events for the statistical analysis. For open ocean waves, reasonable collocation windows are of the order of 1 hour in time and 100 km in space [Monaldo, 1988; Tournadre and Ezraty, 1990].

In practice, the spatial and temporal separation distances and the achievable number of collocation events are restricted by the specific satellite and instrument parameters.

1. The spatial distance between collocated H_s^{swm} and H_s^{ers} data always amounts to 260 km, being fixed by the geometry of the slant-looking SAR with 19.9° incidence angle and by the nadir-looking altimeter. For every H_s^{swm} sample there exists a simultaneously measured H_s^{ers} , yielding at best about 30,000 H_s collocations per month.

2. Collocations of H_s^{swm} and H_s^{top} are achieved whenever the ERS-1 and the TOPEX satellite paths cross within the given space and time windows. This

limits the number of collocations with H_s^{top} to $\sim 1/10$ the number of collocations with H_s^{ers} .

3. The differing orbit inclinations imply variable spatial distributions of the collocations. The ERS-1 is a Sun-synchronous polar orbiting satellite with 98.5° inclination angle; the TOPEX satellite has an altimetric-oceanographic orbit with 66° inclination angle. The ERS-1 satellite records data between latitudes of 81.5° N/S and the TOPEX between 66° N/S. This results in ERS-1 measurements being more homogeneously distributed with latitude, in contrast to the TOPEX measurements being most densely distributed close to the turning latitudes at 66° N/S. Consequently, the TOPEX altimeter measures relatively more frequently high waves from the midlatitude strong westerly wind regions than low waves from the lower wind regions in low latitudes.

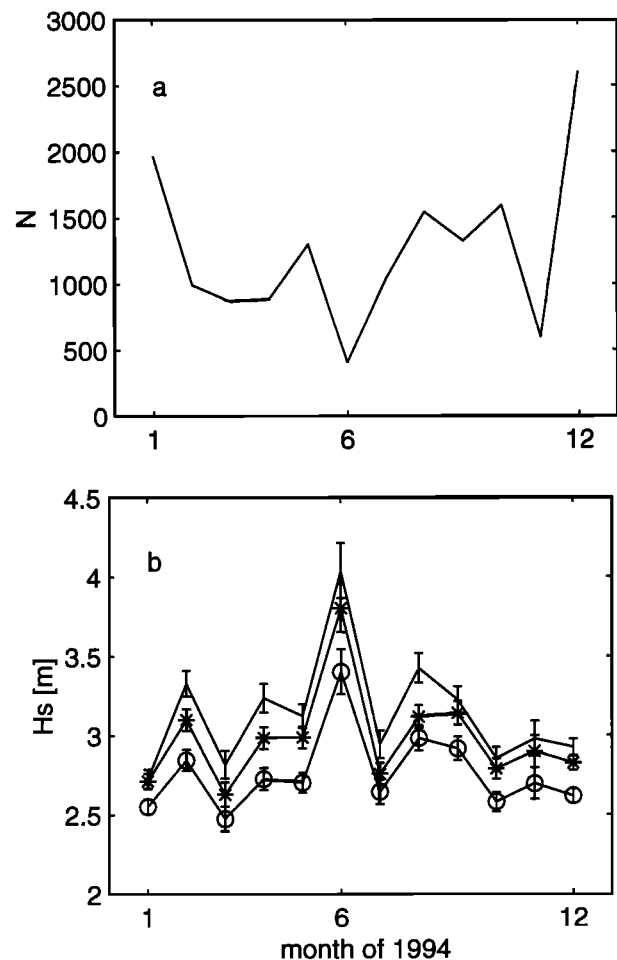


Figure 1. Time series for 1994 of monthly number of (a) samples N and (b) mean H_s from global collocation of H_s from SAR wave mode spectra to H_s from TOPEX altimeter (H_s^{top}) with separation distances up to 260 km and 90 min. The means of H_s^{top} (solid line), of H_s^{swm} (solid line with asterisk), and of H_s from the first-guess of the WAM model (solid line with circle) are shown with error bars indicating the 95% confidence interval.

Thus the global mean values of H_s^{top} are expected to be larger than H_s^{ers} .

To summarize, the spatial and temporal separation of the H_s^{swm} and H_s^{ers} collocations are fixed at 260 km and 0 min. According to this, the distances between the H_s^{swm} and the H_s^{top} collocations are bounded to 260 km and 90 min. We shall see that the correlation between H_s^{swm} and H_s^{top} collocations increases only little when the collocation windows are narrowed. To minimize the differences arising from the different orbit patterns, we limit the ERS-1 data to lie between 66°S and 66°N.

3. Statistical Comparison of H_s Data

3.1. Time Series of Monthly Means

Time series of the global monthly mean significant wave heights reveal H_s^{swm} to be lower than the mean of H_s^{top} (Figure 1) and of H_s^{ers} (Figure 2). The differences between H_s^{swm} and H_s^{top} are insignificant on the 95% confidence level for half of the monthly means, whereas the differences between H_s^{swm} and H_s^{ers} are significant all the time.

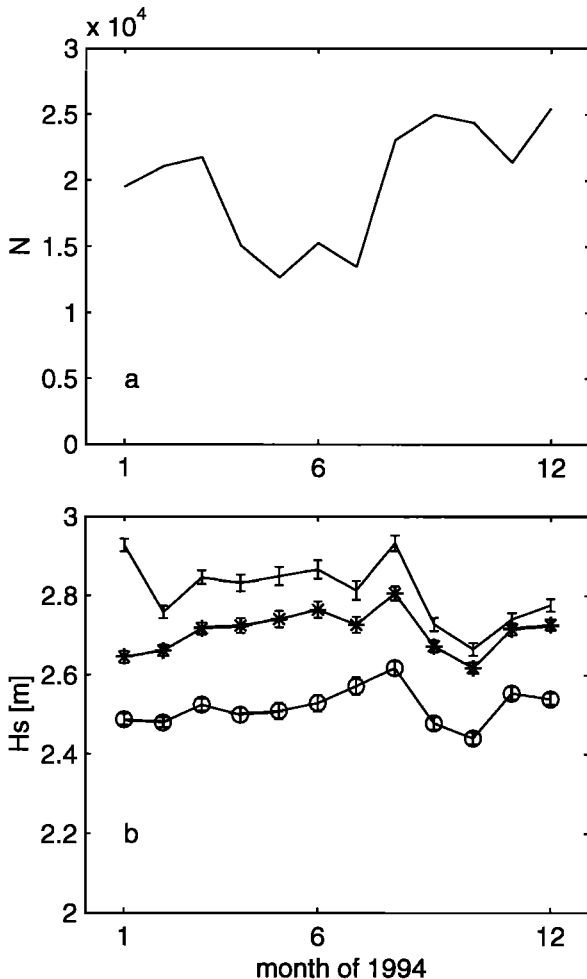


Figure 2. Time series as in Figure 1 but for H_s^{swm} collocated to H_s^{ers} of ERS-1 altimeter with geometry-fixed separation distances of 260 km and 0 min.

For reference, we also display the monthly mean wave heights of the WAM model (H_s^{wam}) in Figures 1 and 2. The monthly means of H_s^{swm} are seen to be always larger, on the 95% confidence level, than the corresponding means of H_s^{wam} with one exception in July 1994 in Figure 1. This leads to two remarks on the first-guess WAM model data: First, the underestimation of (H_s^{wam}) may in part manifest the impact of assimilating H_s^{ers} into the WAM model [Bauer and Staabs, 1998]. The WAM model data incorporate the FD ERS-1 data without correcting the underestimation inherent in these data (see section 2.2). Second, the significantly larger values of H_s^{swm} compared to H_s^{wam} give further evidence that the iterative retrieval algorithm successfully decouples the retrieved spectrum from the first-guess wave spectrum as demonstrated by a synthetic perturbation of the first-guess spectra [Heimbach et al., 1998].

The rather large month-to-month variability which is apparent in the SWM versus TOPEX collocations is largely due to the variable sample sizes and the heterogeneous spatial distributions. The low sample sizes in June and November are caused by data gaps in the H_s^{top} data set (Figure 1). Large data gaps also occur between April and July in the H_s^{ers} data set (Figure 2).

The statistics of the global and monthly H_s data sets are consistent with the statistics of the regional and seasonal data sets. This is found from statistical comparisons (not shown) of regional subsets (northern and southern extratropical and tropical regions of each ocean basin) and of seasonal subsets. More details on the systematic differences between the H_s^{swm} and the collocated altimeter H_s are derived in the following by means of principal component analysis (PCA) [Preisendorfer, 1988; Bauer and Staabs, 1998], the statistics of differences, and the probability density distributions.

3.2. Statistics of Bivariate Data Distributions

The scatter diagrams of the bivariate data distributions of H_s^{swm} against H_s of both altimeters are very similar and show negligible small differences when narrowing the separation distances of collocation. This is inferred from comparing the scatter diagram of the H_s^{swm} versus H_s^{ers} from fixed separation distances of 260 km and 0 min (Figure 3) with the two scatter diagrams of H_s^{swm} versus H_s^{top} from the wide separation window of 260 km and 90 min (Figure 4) and the narrow window of 60 km and 60 min (Figure 5). The narrow window is in accordance with the requirements proposed by Monaldo [1988] and Tournadre and Ezraty [1990].

The statistical parameters (see Appendix) derived from the three collocation sets are presented in Table 1. Although the collocation criteria and the sample sizes among the two H_s^{swm} and H_s^{top} collocation sets differ substantially, the statistical parameters differ hardly.

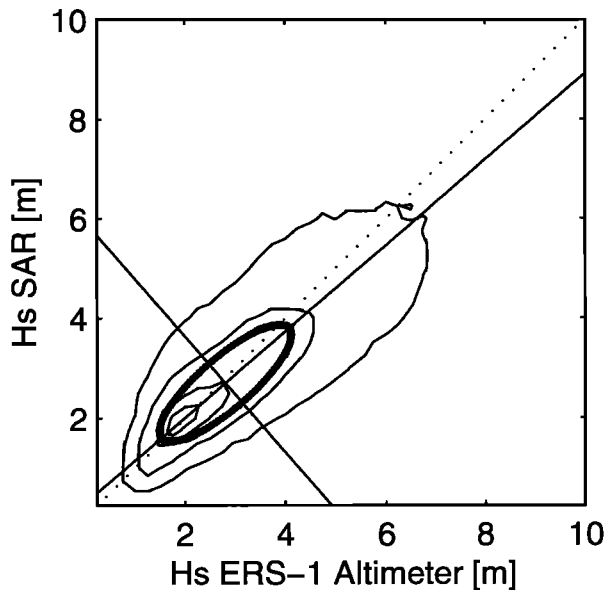


Figure 3. Scatter diagram of H_s^{swm} collocated to H_s^{ers} of 1994 with fixed separation distances (260 km, 0 min) yielding $N=238,000$ samples. The ellipse and its axes are constructed from principal component analysis (compare Appendix). Contour lines enclose 1, 10, 50 and 80% of the number of samples of the modulus of the distribution.

We are therefore confident, that the spatially more distant collocations, particularly of the H_s^{swm} and H_s^{ers} collocations still provide meaningful statistical parameters.

The only marked differences between the collocated sets of H_s^{swm} versus H_s^{top} and of H_s^{swm} versus H_s^{ers} are

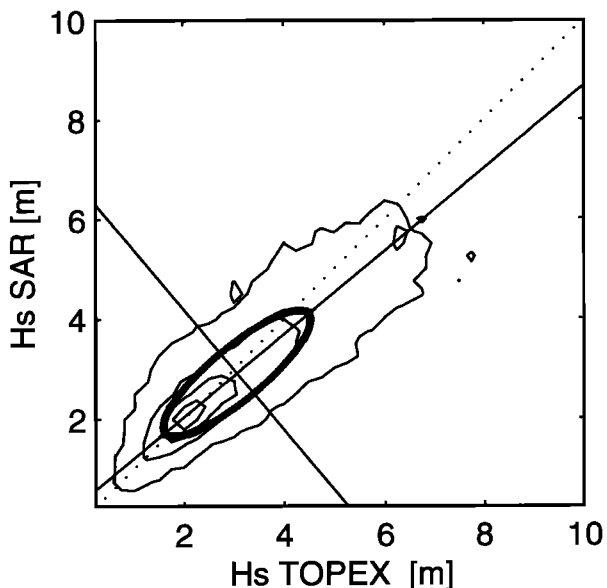


Figure 4. Scatter diagram as in Figure 3 but of H_s^{swm} collocated to H_s^{top} of 1994 with wide separation distances up to 260 km and 90 min yielding $N=15,100$ samples. Contour lines enclose 2, 20, 50 and 80% of the number of samples of the modulus of the distribution.

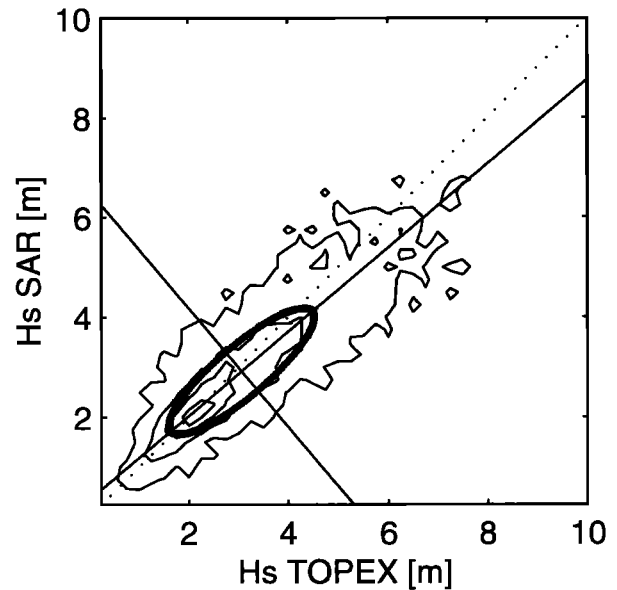


Figure 5. Scatter diagram as in Figure 4 but with narrow separation distances up to 60 km and 60 min from $N=2498$ samples. Contour lines as in Figure 4.

the mean values and the variabilities along the major principal axes. The mean of H_s^{top} exceeds the mean of H_s^{ers} by 0.25 m; the major principal rms deviation σ_{p1} of H_s^{swm} versus H_s^{top} is 0.2 m larger than for H_s^{swm} versus H_s^{ers} . These differences are to be ascribed to the different spatial sampling properties of the ERS-1 and TOPEX altimeter described earlier.

As already revealed from the monthly means, the annual mean of H_s^{swm} is too low. This underestimation amounts to 0.10 m or 5% with respect to H_s^{ers} , as inferred from the slope $b_{0\text{pca}}$ of the major axis passing through the origin, and to 0.13 m or 6% with respect to H_s^{top} . However, the major principal axis indicates that only the high waves of H_s^{swm} are underestimated, whereas the low waves are overestimated. Compared to the uncorrelated scatter of $\sigma_{p2} = 0.5$ m, the mean underestimation may be regarded small. The uncorrelated error determined between H_s^{swm} and H_s of the altimeters is the same as between H_s^{swm} and H_s^{wam} and is about 0.1 m larger than found by *Bauer and Staabs* [1998]. This suggests that the extra scatter here is due to the reduced smoothing effect implied by the three-point average of the altimeter data compared to the 30-point average by *Bauer and Staabs* [1998].

3.3. Statistics of Differences

The differences of H_s^{swm} with respect to H_s of the altimeter are seen to depend on wave height. This follows from the partial bias as function of wave height, i.e., the bias between SWM-retrieved and altimeter H_s computed for wave height intervals and also from the partial relative bias, i.e., the partial bias weighted with the corresponding mean of the altimeter H_s . The partial bias is positive for H_s less than 2 m and becomes

Table 1. Statistical Comparison of SWM- H_s Globally Collocated to ERS-1 Altimeter- H_s With Fixed Separation Distance (260 km, 0 min) and of SWM- H_s Globally Collocated to TOPEX Altimeter- H_s With Wide (260 km, 90 min) and Narrow Separation Distances (60 km, 60 min) for 1994

Separation	$H_s^{\text{swm}}/H_s^{\text{ers}}$	$H_s^{\text{swm}}/H_s^{\text{top}}$	$H_s^{\text{swm}}/H_s^{\text{top}}$
	Fixed	Wide	Narrow
N	238,315	15,131	2498
$\langle H_s^{\text{swm}} \rangle$	2.71 ± 0.01	2.92 ± 0.02	2.92 ± 0.05
bias	-0.10	-0.14	-0.14
rms dev	0.74	0.79	0.75
r	0.83	0.85	0.86
b_{pca}	0.86	0.83	0.84
a_{pca}	0.29	0.38	0.34
$b_{0\text{pca}}$	0.95	0.93	0.94
σ_{p1}	1.69	1.87	1.87
σ_{p2}	0.51	0.52	0.50

The statistical parameters are: $\langle H_s^{\text{swm}} \rangle$ = mean of SWM- H_s with 95% interval, bias of $H_s^{\text{swm}} - H_s$ of altimeter, rms dev = square root of the deviation of the differences, correlation coefficient r , slope b_{pca} and intercept a_{pca} of the major principal axis, slope $b_{0\text{pca}}$ of the major principal axis tied to the origin, and principal rms deviations σ_{p1} and σ_{p2} along the major and minor axis, respectively (see Appendix). Units are m.

gradually negative beyond 2 m (Figure 6a). The partial relative bias decreases from more than 30% for low waves to about -20% for high waves (Figure 6b). The standard deviation of the differences associated with the partial bias, which is shown by error bars in Figure 6a, is quite large and grows with wave height. From this the partial bias may be regarded not significantly different from zero for low-to-moderate waves, but the underestimation of the high H_s^{swm} needs a closer inspection.

We define extreme deviations as being larger than 4 m. From the H_s^{swm} collocations about 0.1–0.2% deviate extremely from H_s of the altimeters of which 70% of H_s^{swm} are biased low and 30% are biased high. Extreme underestimations of H_s^{swm} are found predominantly during winter in the midlatitude high wind regions (between $\sim 40^\circ$ and 66° latitude), whereas overestimations appear randomly distributed in time and latitude (Figure 7). Different reasons for the large deviations are conceivable.

1. In the most southern region, erroneous measurements may be obtained due to the occurrence of sea ice. Such cases might not have been adequately filtered out because of inaccuracies in determining the ice distributions for the WAM model grid. The errors in the measurements would result from the selective damping of waves and the disturbances from solid ice edges which influence both the SAR and the altimeter measurements. Consequently, both the SWM and the altimeter data sets might contain erroneous measurements. In addition to relying on the sea ice maps, as

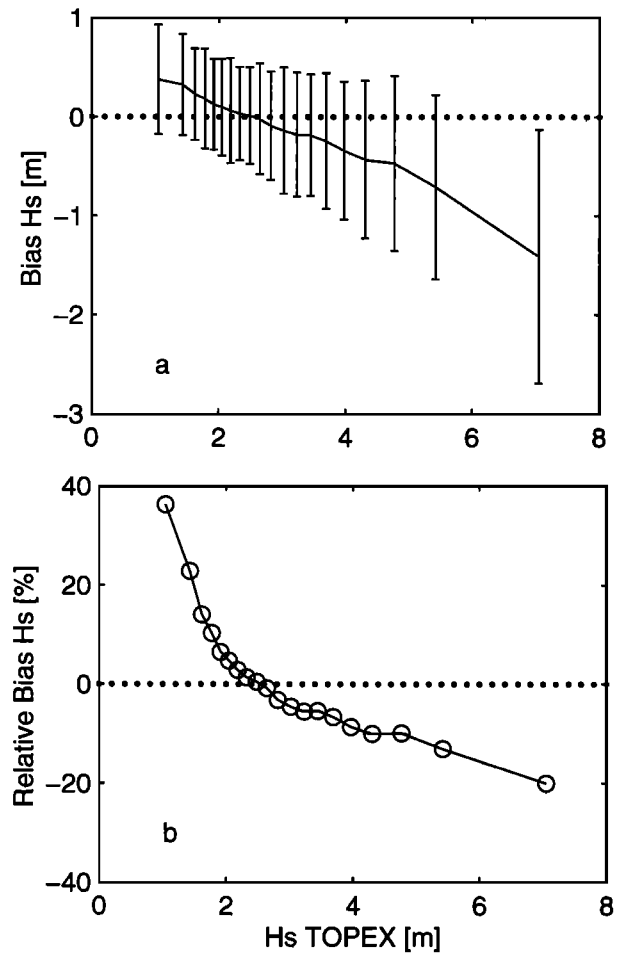


Figure 6. (a) Wave height depending bias = $H_s^{\text{swm}} - H_s^{\text{top}}$ with error bars for 95% confidence interval and (b) relative bias = $(H_s^{\text{swm}} - H_s^{\text{top}})/H_s^{\text{top}}$ as function of H_s^{top} with collocation distances up to 260 km and 90 min.

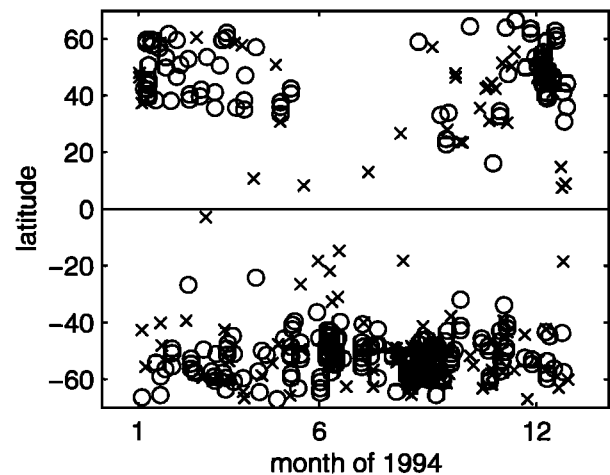


Figure 7. Time-latitude distribution of the H_s^{swm} versus H_s^{ers} collocations of which H_s^{swm} deviates extremely (> 4 m) from H_s^{ers} , which applies to about 0.1% of the data. 70% of these represent underestimations of H_s^{swm} , marked with circles, and 30% represent overestimations, marked with crosses.

inferred from daily NCEP sea surface temperature analyses, we could have used the weekly polar sea ice maps directly inferred from ERS-1 scatterometer data which have recently become available from the French ERS processing and archiving facility CERSAT/IFREMER [e.g., Gohin, 1995; Ezraty *et al.*, 1996]. However, since most of the problematic data are found well away from the expected sea ice boundary, only very little improvement is to be expected using also the weekly ice maps.

2. The simulation of the first-guess spectrum might be incorrect due to incorrect wind forcing. Comparing mean wind speeds of the ECMWF model and of the ERS-1 scatterometer of 1994, the former are seen to be overestimated in the northern extratropical regions and to be considerably underestimated south of 55°S [Bentamy, 1996, 1997]. This could imply underestimations of the modeled wave heights in the north and overestimations in the far south. However, the locations of extreme deviations of both signs are quite evenly distributed on both hemispheres (Figure 7). Obviously, the extreme deviations are not related to erroneous first-guess estimates, confirming the results of Heimbach *et al.* [1998].

3. The retrieval algorithm might be suspected to have shortcomings, for instance, due to the azimuthal cutoff in the measured backscatter. However, the frequency distribution of the azimuth angle (i.e., angle between the wave propagation and the satellite flight direction) of the underestimated H_s^{swm} shows hardly any occurrence of azimuthally traveling waves (Figure 8) although azimuthally waves occur relatively often. The extreme H_s^{swm} underestimations are most frequent for waves traveling 30° off the range direc-

tion. In general, range traveling waves occur most often. Only a small fraction of these contribute to cases of extreme H_s^{swm} underestimations. This suggests that range traveling waves are relatively more often correctly estimated. However, cases of extreme H_s^{swm} overestimations, which are rare, refer relatively more often to range traveling waves (not shown). Thus detailed case studies are necessary for a proper interpretation.

In summary, each of the potential causes considered for the large deviations can only explain a fraction of the deviations. Neither a single reason nor a systematic error source can be identified to be responsible for the deviations. The deviations appear to contain a considerable fraction of random uncertainties. This is suggested from the relatively large uncorrelated scatter ($\sigma_{p2} = 0.5$ m) which is the same for all possible collocations among H_s^{swm} , H_s^{ers} , H_s^{top} and H_s^{wam} . Finding the causes for the systematic underestimation is hampered by the fact that H_s is very often composed of wind sea and swell contributions which may contain different errors. This led us to validate H_s^{swm} in more simple cases in which H_s^{swm} consists of either wind sea or swell only (see section 3.5).

3.4. Comparison of Probability Distributions

A relative measure of the quality of H_s data sets is the consistency of the H_s data distribution with the lognormal (GNO) and the generalized extreme value (GEV) distribution [Bauer and Staabs, 1998]. These two parametric distributions have been found empirically among the basic distribution functions, as for instance presented by Hosking [1990], to suitably approximate the mean, the modus, and the tails of measured and modeled H_s data sets. Cases for which H_s distributions deviate significantly from these parametric distributions are generally associated with deficiencies in the data. Therefore the parametric distributions are valuable means to assess the quality of the H_s distributions.

The histograms of H_s^{swm} and of H_s^{top} from the narrow collocation (60 km, 60 min) in Figures 9 and 10, respectively, depict the fitted GNO (dashed curve) and GEV (solid curve) probability density function. The ensembles are not sufficiently large ($N=2498$) for obtaining smooth frequency distributions. Nevertheless, the distributions of the collocated H_s^{swm} and H_s^{top} agree remarkably well.

The histograms of the collocated H_s^{swm} and H_s^{ers} are shown in Figures 11 and 12, respectively. These histograms differ slightly, with the mean of H_s^{swm} being 0.1 m lower and the modus being 0.2 m higher than from H_s^{ers} . Note that the histogram of H_s^{swm} represents a smooth unimodal distribution, whereas the histogram of H_s^{ers} shows an unusual indentation between 2 and 3 m with respect to the parametric distributions. This is in line with previous results of Bauer and Staabs [1998] and indicates that FD H_s of ERS-1 may need preferably

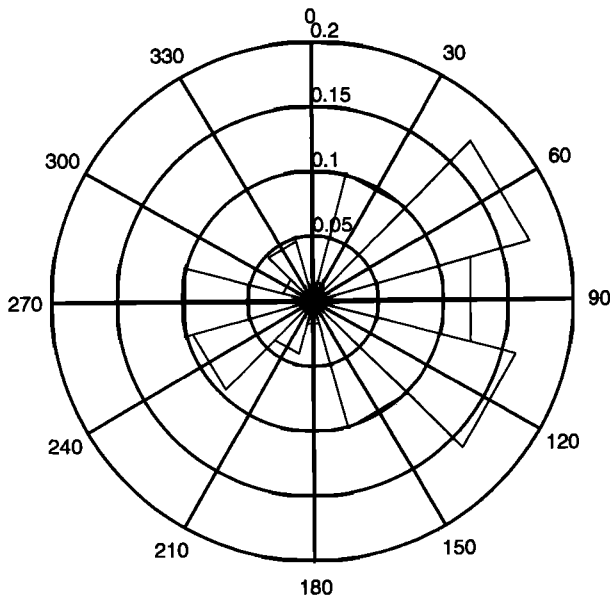


Figure 8. Relative frequency distribution of azimuth angle determined from those cases only, for which H_s^{swm} is underestimated by more than 4 m with respect to collocated H_s^{ers} .

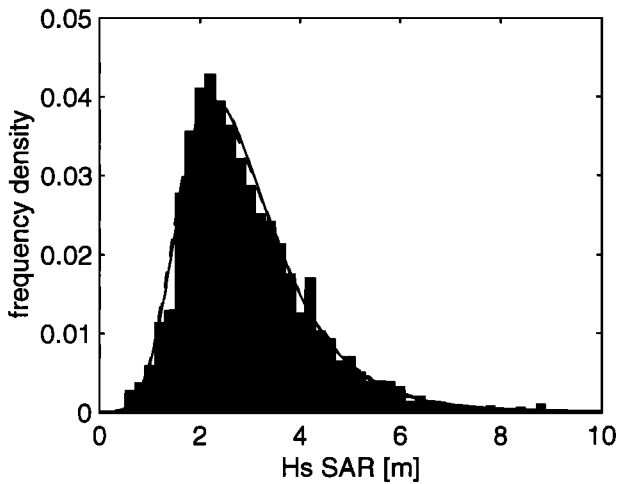


Figure 9. Histogram of H_s^{swm} with fitted GEV (solid) and GNO (dashed) distribution function from collocation to H_s^{top} within separation distances up to 60 km and 60 min ($N=2498$).

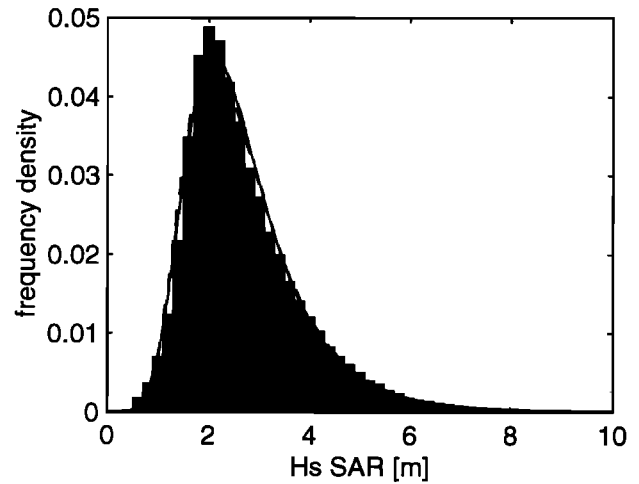


Figure 11. Histogram of H_s^{swm} with fitted GEV (solid) and GNO (dashed) distribution function from collocation to H_s^{ers} based on $N= 238,315$.

a nonlinear correction rather than a linear correction as applied here.

We observe that the SWM-retrieved H_s match the parametric distribution curves very well; in fact, the distances between the H_s^{swm} histograms and the distribution curves are smaller than the corresponding distances derived from the histograms of the altimeter data. In view of the different mapping regimes of the nonlinear spectral wave-to-SAR transform for low and high sea states this was not obvious and therefore represents a further confirmation of the reliability of the retrieval algorithm. The slight overshoot at the peak of the H_s^{swm} histograms compared to the peak of the parametric distributions is apparent also from the histograms of H_s^{top} and H_s^{ers} . This points to a relative oversampling of H_s data close to the mean value of 2 m which was not

observed when H_s were sampled globally without applying any sampling criteria as in the work of *Bauer and Staabs* [1998].

4. Comparison of H_s of Pure Wind Sea and Swell

Previous results showed that the correspondence of ERS-1 SWM spectral retrievals with WAM model spectra depends on the contributions of wind sea and swell [*Heimbach et al.*, 1998]. On average, the SWM wind sea wave height was found to be lower than the modeled wind sea wave height. In contrast, the SWM swell wave height tended to become gradually larger relative to the modeled swell wave height in the progress of wave decay and wave propagation. In other words, the swell wave height modeled by the WAM model was seen to

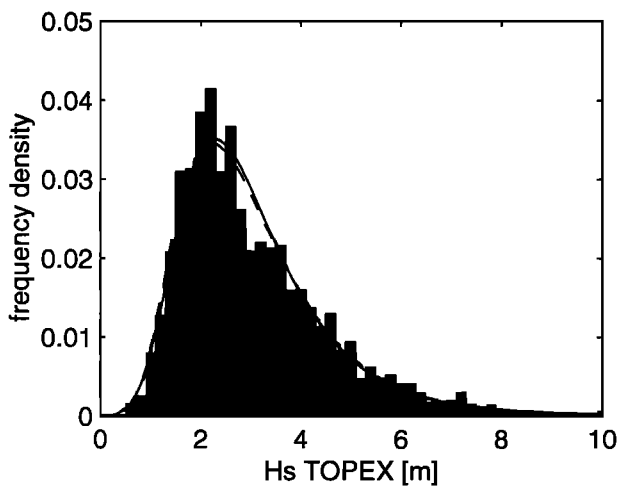


Figure 10. Histogram of H_s^{top} corresponding to Figure 9.

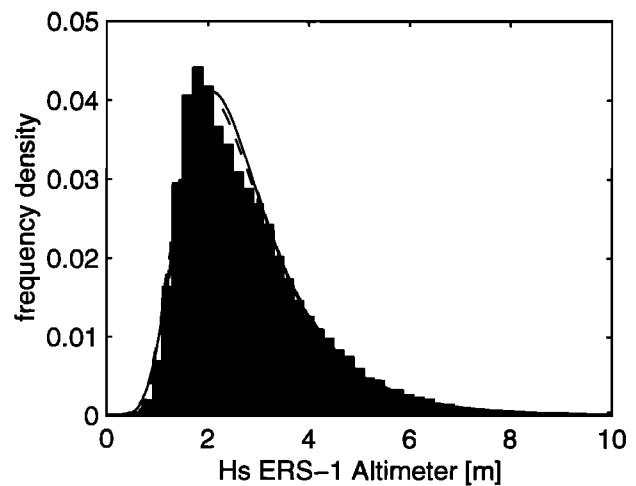


Figure 12. Histogram of H_s^{ers} corresponding to Figure 11.

be increasingly underestimated with increasing spectral wave age. (The spectral wave age denotes the time interval which has passed since the waves experienced the last active forcing.)

To estimate any possible distinct behavior of wind sea and swell from total H_s , alone we have isolated two sets of spectra, one representing spectra that only contain a wind sea system and the other representing spectra that contain only (one or several) swell systems. Wind sea and swell systems are identified by means of the spectral partitioning algorithm [Hasselmann *et al.*, 1996] in conjunction with the local wind vector, which in our case is obtained from the ECMWF analysis. The wind sea wave height is determined from the integral over that coherent fraction of the spectral wave energy density which is influenced by the local wind. The local wind is said to have influence, if the wind is aligned with the direction of the energy density fraction, and if the peak phase speed is less than 1.3 times the wind speed component in the wave propagation direction. Most of the remaining spectral energy is considered as swell energy, with a tiny residual attributed to mixed wind sea/swell.

The H_s values of these two subsets of the SWM retrievals and their collocated altimeter data provide estimates of pure wind sea and pure swell wave heights. The collocated sets of wind sea and swell for 1994 are presented by scatter diagrams. The spatial and the temporal separation distance for TOPEX versus SWM swell cases is set to 60 km and 60 min and for the TOPEX versus SWM wind sea cases to 30 km and 30 min. The smaller separation distances for the wind sea cases accounts for the fetch and duration effects and thus slightly reduce the scatter.

The swell wave heights of H_s^{swm} agree very well with the collocated wave heights of H_s^{ers} (Figure 13) and of

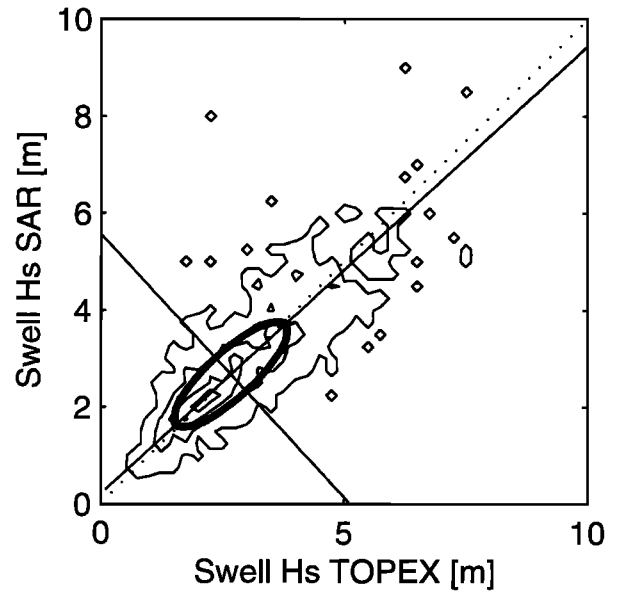


Figure 14. Scatter diagram as in Figure 5 but for pure of swell H_s^{swm} collocated to H_s^{top} based on $N=869$. Contour lines as in Figure 4.

H_s^{top} (Figure 14). The swell wave heights range up to 7 m, and the slopes of the major axes are very close to 1. Associating high (low) waves with young (old) waves as a first rough estimate, the agreement may be considered invariant with respect to wave age.

The number of cases of pure wind sea systems is much smaller compared to the number of swell cases. The pure wind sea H_s range from 0.5 to almost 10 m. The pure wind sea wave heights of H_s^{swm} are considerably lower than of H_s^{ers} (Figure 15) and of H_s^{top} (Figure 16). The slopes of the major axes through the origin indicate

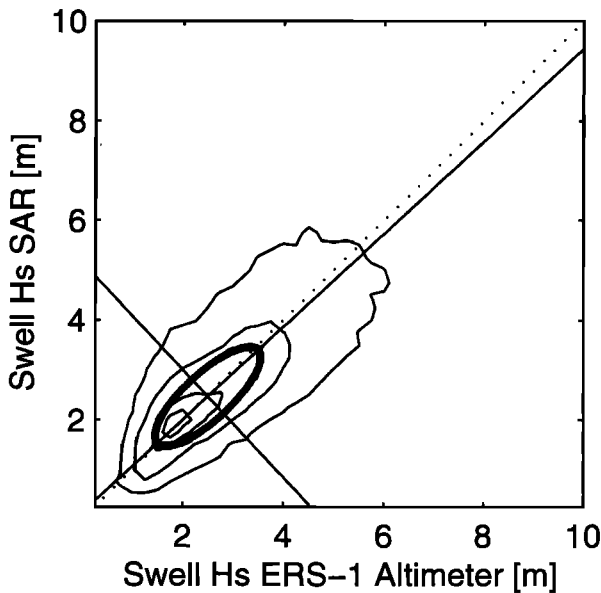


Figure 13. Scatter diagram as in Figure 3 but for pure swell H_s^{swm} collocated to H_s^{ers} based on $N=81,600$. Contour lines as in Figure 3.

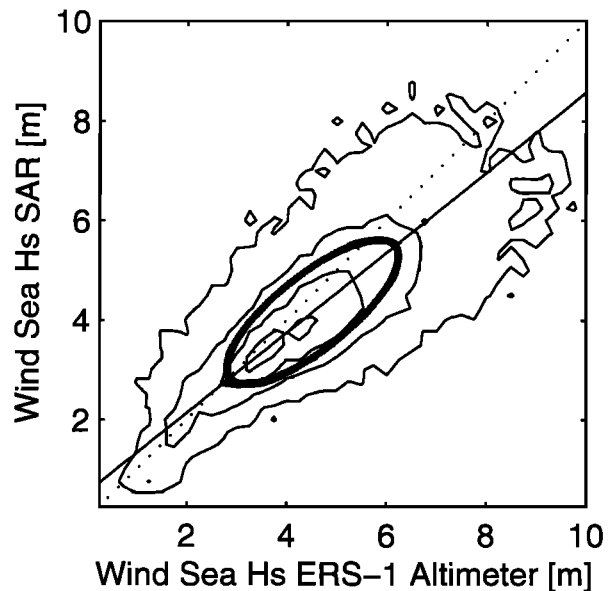


Figure 15. Scatter diagram as Figure 3 but for pure wind sea H_s^{swm} collocated to H_s^{ers} based on $N=15,900$. Contour lines as in Figure 4.

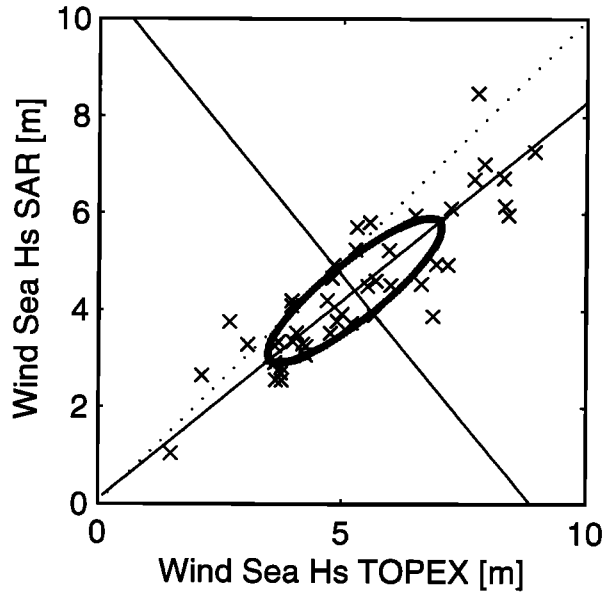


Figure 16. Scatter diagram as figure 5 but for pure wind sea H_s^{swm} collocated to H_s^{top} based on $N=46$ samples and small separation distances of up to 30 km and 30 min.

an underestimation by 9% with respect to wind sea of H_s^{ers} and by even 16% with respect to H_s^{top} . The uncorrelated error is larger for the wind sea collocations with H_s^{ers} (0.74 m) than for those with H_s^{top} (0.58 m) mainly because the scatter of the wind sea collocations decreases with decreasing spatial and temporal separation distances.

Table 2 summarizes the statistical comparison of H_s^{swm} versus H_s^{top} collocations and the extracted collocations consisting of pure wind sea and pure swell. The underestimation of H_s^{swm} is visible only in the wind sea but not in the swell cases. As depicted in Figure 7 for total H_s^{swm} , the underestimation of the wind sea H_s^{swm} accumulates in the high wind regions and vanishes in the northern latitudes during summer.

Further investigations on both the altimeter and the SWM data sets are needed, for which the stratification of the data with respect to wind sea and swell or other spectral properties are very helpful, to identify causes for the deviations and to explain the remaining inconsistencies.

5. Conclusions

A comprehensive validation of global H_s retrieved from ERS-1 SAR wave mode spectra (H_s^{swm}) during 1994 is performed using independent, buoy-validated measurements of the altimeters onboard the TOPEX/Poseidon (H_s^{top}) and ERS-1 (H_s^{ers}) satellites. This provides an absolute assessment of the validity of H_s^{swm} which complements the extensive assessment of the SWM raw data quality, the retrieval algorithm performance, and the relative SWM to WAM spectral inter-

comparison of a 3-year global SWM and WAM spectral data set [Heimbach *et al.*, 1998]. The present validation refers to universal statistical properties of H_s data inferred from different spaceborne altimeters, from in situ data, and from wave modeling [Bauer and Staabs, 1998].

Considering the entirely different complexity of the data processing schemes to retrieve H_s from the SWM imagerie spectrum and from the shape of the altimeter pulse, the overall agreement between the instantaneous H_s collocations is remarkably good. In particular, the low-to-moderate H_s data of the SWM retrievals correspond closely to altimeter H_s . The close correspondence between H_s^{swm} and altimeter-derived H_s for the dominant range of wave heights is overshadowed by the relatively large uncorrelated rms error of 0.5 m. This scatter hardly diminishes by narrowing the spatial and temporal distances between the collocated data. Apparently, individual shortcomings of the different data processing schemes add together. In this study, the most obvious lines of agreements and shortcomings are described leading to the following conclusions:

1. The separate validation of SWM-retrieved wind sea and swell wave data is valuable to assess their applicability for evaluating the corresponding spectral properties obtained with the WAM model. The collocated data of H_s^{swm} and H_s^{top} representing pure swell waves agree very closely, which is manifested by a slope of 0.99 of the major axis of the data distribution. Thus SWM-retrieved swell wave heights may be considered to be of good absolute quality and are suitable for improving the modeling of swell waves which often appear to be too low.

2. In contrast to the high absolute quality of the moderate wave heights the high sea states retrieved from the SWM spectra associated to wind sea are signif-

Table 2. Statistical Comparison of SWM- H_s Globally Collocated to TOPEX Altimeter- H_s for 1994 With Separation Distance up to 60 km, 60 min, and for Subset of Pure Swell Waves (Separation Distance up to 60 km, 60 min), and Pure Wind Sea Waves (Separation Distances up to 30 km, 30 min), As Inferred From SWM Spectral Retrievals

Separation	H_s	Swell H_s	Wind Sea H_s
	60 km, 60 min	60 km, 60 min	30 km, 30 min
N	2498	869	46
$\langle H_s^{\text{swm}} \rangle$	2.92 ± 0.05	2.67 ± 0.07	4.41 ± 0.43
$\langle H_s^{\text{top}} \rangle$	3.06 ± 0.05	2.67 ± 0.08	5.26 ± 0.51
r	0.86	0.83	0.87
b_{pca}	0.84	0.92	0.82
a_{pca}	0.34	0.21	-0.07
$b_{0\text{pca}}$	0.94	0.99	0.84
σ_{p1}	1.87	1.52	2.25
σ_{p2}	0.50	0.47	0.58

For further explanations see Table 1.

icantly too low. The underestimation of SWM wind sea wave heights with respect to TOPEX altimeter H_s is up to 16% with an uncorrelated error of 0.6 m. As has been shown, this relatively large scatter cannot simply be attributed to uncertainties in the SWM retrievals. The same scatter arises from the collocations between the altimeter data H_s^{top} and the H_s^{ers} . This suggests that a significant contribution to the scatter originates also from the uncertainty of the altimeter measurements. The systematic underestimation of the high sea states by H_s^{swm} with respect to H_s^{top} can neither solely be attributed to errors induced by the occurrence of sea ice nor to the loss of information caused by the azimuthal cutoff in the SAR measurements or to erroneous first-guess spectra applied in the retrieval algorithm.

3. It is demonstrated that the SWM data are useful also to analyze shortcomings of the altimeter data. The histograms of collocated H_s^{swm} and H_s^{top} show a closer correspondence than the histograms of H_s^{swm} and H_s^{ers} . This confirms the results that partly the H_s^{ers} causing the misfit [e.g., *Bauer and Staabs*, 1998] which might be sorted out with the help of spectral wave data from SWM.

In summary, the low-to-moderate waves dominated by swell retrieved from SWM spectra are shown to be of high absolute quality, whereas high sea states are occasionally significantly underestimated. The best way to find the causes for the deviations is the joint analysis of the measured and modeled wave spectra through a dynamically consistent wave data assimilation system together with the analysis of modeled and measured wind data. It is a major challenge to sort out the remaining inconsistencies in order to obtain a high-quality spectral wave data set for wave research and applications. The wave observations from ERS-1 and ERS-2 and from the forthcoming ENVISAT, scheduled for the year 1999, will provide more valuable information and contribute to improve spectral wave data for global wave prediction and wave climate research.

Appendix

The principal components are defined by the first and second eigenvalue of the data covariance matrix [e.g., *Preisendorfer*, 1988]. The eigenvalues $\sigma_{p1,p2}^2$ are equivalent to the variances along the major and the minor principal axes, respectively. The principal variances are

$$\left. \begin{matrix} \sigma_{p1}^2 \\ \sigma_{p2}^2 \end{matrix} \right\} = \frac{1}{2} \left\{ (s_{xx} + s_{yy}) \pm [(s_{xx} - s_{yy})^2 + 4s_{xy}^2]^{\frac{1}{2}} \right\} \quad (2)$$

where σ_{p1}^2 (σ_{p2}^2) is computed with plus (minus) sign, and s_{xx} and s_{yy} denote the variances of the x and the y variable, respectively, and s_{xy} denotes the covariance. The variance σ_{p1}^2 represents the effective variance and σ_{p2}^2 the uncorrelated variance of the two data sets, where each data set has random uncertainties. The

ratio σ_{p1}/σ_{p2} may be interpreted as a measure of the signal-to-noise ratio. The agreement between two collocated data sets may be called perfect if the major principal axis is aligned with the diagonal of the scatter diagram and if the minor variance vanishes. The slope and the intercept of the major principal axis are denoted b_{pca} and a_{pca} , respectively. The major axis passing through the origin with slope b_{0pca} is inferred by using the uncentered variances without subtracting the means.

Acknowledgments. The study contributes to the ESA Pilot Project PP2-D1 "Derivation and assimilation of ERS-1 wind and wave data," and receives funding by the BMBF project 03F0185A. We are indebted to C. Staabs for helping with the altimeter data, and we are grateful for discussions with S. and K. Hasselmann.

References

- Alpers, W., and K. Hasselmann, The two-frequency microwave technique for measuring ocean wave spectra from an airplane or satellite, *Boundary Layer Meteorol.*, **13**, 215-230, 1978.
- Alpers, W., and K. Hasselmann, Spectral signal-to-clutter and thermal noise properties of ocean wave imaging synthetic aperture radars, *Int. J. Remote Sens.*, **3**, 423-446, 1982.
- Alpers, W., D.B. Ross, and C.L. Rufenach, On the detectability of ocean surface waves by real and synthetic aperture radar, *J. Geophys. Res.*, **86**, 6481-6498, 1981.
- Alpers, W., C. Brüning, and K. Richter, Comparison of simulated and measured synthetic aperture radar image spectra with buoy-derived ocean wave spectra during the Shuttle Imaging Radar-B mission, *IEEE Trans. Geosci. Remote Sens.*, **24**, 559-566, 1986.
- Bacon S., and D. J. T. Carter, Wave climate changes in the North Atlantic and North Sea, *Int. J. Climatol.*, **11**, 545-558, 1991.
- Bauer, E., and C. Staabs, Statistical properties of global significant wave heights and their use for validation, *J. Geophys. Res.*, **103**, 1153-1166, 1998.
- Bauer, E., K. Hasselmann, I.R. Young, and S. Hasselmann, Assimilation of wave data into the wave model WAM using an impulse response function method, *J. Geophys. Res.*, **101**, 3801-3816, 1996.
- Bauer, E., S. Hasselmann, P. Lionello, and K. Hasselmann, Comparison of assimilation results from an optimal interpolation and the Green's function method using ERS-1 SAR wave mode spectra, in *Proceedings of the Third ERS Scientific Symposium*, Florence, Italy, 17-20 March 1997, *ESA SP-414*, pp. 1131-1136, Eur. Space Agency, Paris, 1997.
- Bauer, E., H. von Storch, and M. Stolley, Sensitivity of ocean waves to speed changes of the weather stream, *Global Atmos. Ocean Syst.*, in press, 1999.
- Beal, R.C. (Ed.), Directional ocean wave spectra, The Johns Hopkins Univ. Press, Baltimore 1991.
- Bentamy, A., N. Grima, Y. Quilfen, V. Harscoat, C. Maroni, and S. Pouliquen, An atlas of surface wind from ERS-1 scatterometer measurements 1991 - 1996, *IFREMER publ., DRO/OS, BP 70*, Inst. Fr. de Rech. pour l'Exploit. de la Mer, Plouzané, France, 1996.
- Bentamy, A., et al., Wind climatology from ERS scatterometer, in *Proceedings of the Third ERS Scientific Symposium*, Florence, Italy, 17-20 March 1997, *ESA SP-414*, pp. 1181-1186, Eur. Space Agency, Paris, 1997.

- Brüning, C., W. Alpers, L.F. Zambresky, and D.G. Tilley, Validation of a SAR ocean wave imaging theory by the Shuttle Imaging Radar-B experiment over the North Sea, *J. Geophys. Res.*, *93*, 15,403-15,425, 1988.
- Brüning, C., S. Hasselmann, K. Hasselmann, S. Lehner, and T. Gerling, First evaluation of ERS-1 synthetic aperture radar wave mode data, *Global Atmos. Ocean Syst.*, *2*, 61-98, 1994.
- Callahan, P.S., C.S. Morris, and S.V. Hsiao, Comparison of TOPEX/POSEIDON σ_0 and significant wave height distributions to GEOSAT, *J. Geophys. Res.*, *99*, 25,015-25,024, 1994.
- Cotton, P.D., and D.J.T. Carter, Cross calibration of TOPEX ERS-1, and GEOSAT wave heights, *J. Geophys. Res.*, *99*, 25,025-25,033, 1994.
- European Space Agency (ESA), ERS user handbook, *ESA SP-1148*, ESTEC, Noordwijk, Neth., 1993.
- European Space Agency (ESA), Application achievements of ERS-1, *ESA SP-1176/II*, ESRIN, Frascati, Italy, 1996.
- Ezraty, R., F. Gohin, P. Bryère, C. Maroni, and A. Cavanié, Determination of sea ice extent and ice types using the AMI-wind, Antarctica, 1992-1995, in *Proceedings of the Second ERS Applications Workshop*, London, UK, 6-8 December 1995, *ESA SP-383*, 215-217, Eur. Space Agency, Paris, 1996.
- Gohin, F., Some active and passive microwave signatures of Antarctic sea ice from mid-winter to spring 1991, *Int. J. Remote Sens.*, *16*, 2031-2054, 1995.
- Gower, J.F.R., Intercalibration of wave and wind data from TOPEX/POSEIDON and moored buoys off the west coast of Canada, *J. Geophys. Res.*, *101*, 3817-3829, 1996.
- Grand Banks, The Grand Banks ERS-1 SAR Wave Spectra Validation Experiment, *Atmos. Ocean*, *32*(1), 3-256, 1994.
- Günther, H., S. Hasselmann and P.A.E.M. Janssen, WAModel Cycle 4 (revised version), *Tech. Rep. 4*, Ger. Clim. Comput. Cent. (DKRZ), Hamburg, Germany, 1992.
- Gulev, S.K., D. Cotton, and A. Sterl, Intercomparison of the North Atlantic wave climatology from voluntary observing ships, satellite data and modelling, *Phy. Chem. Earth*, *23*, (5/6), 587-592, 1998.
- Hasselmann, K., and S. Hasselmann, On the nonlinear mapping of an ocean wave spectrum into a synthetic aperture radar image spectrum and its inversion, *J. Geophys. Res.*, *96*, 10,713-10,729, 1991.
- Hasselmann, K., R.K. Raney, W.J. Plant, W. Alpers, R.A. Shuchman, D.R. Lyzenga, C.L. Rufenach, and M.J. Tucker, Theory of synthetic aperture radar ocean imaging, A MARSEN view, *J. Geophys. Res.*, *90*, 4659-4686, 1985.
- Hasselmann, S., C. Bünning, K. Hasselmann and P. Heimbach, An improved algorithm for the retrieval of ocean wave spectra from SAR image spectra, *J. Geophys. Res.*, *101*, 16,615-16,629, 1996.
- Hasselmann, S., P. Lionello and K. Hasselmann, An optimal interpolation assimilation scheme for wave data, *J. Geophys. Res.*, *102*, 16615-16629, 1997.
- Hasselmann, S., P. Heimbach and C. Bennefeld, The WASAR algorithm for retrieving ocean wave spectra from SAR image spectra, *Tech. Rep. 14*, Ger. Clim. Comput. Cent. (DKRZ), Hamburg, Germany, 1998.
- Hasselmann, S., et al., WAMDI Group, The WAM model - A third generation ocean wave prediction model, *J. Phys. Oceanogr.*, *14*, 1775-1810, 1988.
- Heimbach, P., S. Hasselmann, and K. Hasselmann, Statistical analysis and WAM model intercomparison of wave spectral retrievals for a 3 year period of global ERS-1 SAR wave mode, *J. Geophys. Res.*, *103*, 7931-7978, 1998.
- Hosking, J. R. M., L-moments: Analysis and estimation of distributions using linear combinations of order statistics, *J. R. Statist. Soc. B*, *52*, 105-124, 1990.
- Janssen, P.A.E.M., B. Hansen, and J. Bidlot, Verification of the ECMWF wave forecasting system against buoy and altimeter data, *ECMWF Tech. Memo. 229*, Reading, Eng., 1996.
- Kushnir, Y., V.J. Cardone, J.G. Greenwood, and M.A. Cane, The recent increase in North Atlantic wave heights, *J. Clim.*, *10*, 2107-2113, 1997.
- Lionello, P., H. Günther, and B. Hansen, A sequential assimilation scheme applied to global wave analysis and prediction, *J. Mar. Res.*, *6*, 87-107, 1995.
- Monaldo, F., Expected differences between buoy and radar altimeter estimates of wind speed and significant wave height and their implications on buoy-altimeter comparisons, *J. Geophys. Res.*, *93*, 2285-2302, 1988.
- Monaldo, F.M., and D.R. Lyzenga, On the estimation of wave slope- and height variance spectra from SAR imagery, *IEEE Trans. Geosci. Remote Sens.*, *24*, 543-551, 1986.
- Plant, W. J., and W. Alpers, An introduction to SAXON-FPN, *J. Geophys. Res.*, *99*, 9699-9703, 1994.
- Preisendorfer, R. P., *Principal Component Analysis in Meteorology and Oceanography*, 422 pp., Elsevier, New York, 1988.
- Queffelec, P., Significant wave height and backscatter coefficient at ERS-1/2 and TOPEX/POSEIDON ground-track crossing points, FDP, IFREMER contribution to the ERS-2 radar altimeter commissioning phase, *IFREMER Tech. Rep.*, *IFREMER, DRO/OS, BP 70*, 25 pp., Plouzané, France, 1996.
- Tournadre, J., and R. Ezraty, Local climatology of wind and sea state by means of satellite radar altimeter measurements, *J. Geophys. Res.*, *95*, 18,255-18,268, 1990.
- von Storch, H., et al., WASA Group, Changing waves and storms in the Northeast Atlantic? *Bull. Am. Meteorol. Soc.*, *79*, 741-760, 1998.

E. Bauer, Potsdam Institute for Climate Impact Research, Telegrafenberg, 14473 Potsdam, Germany. (bauer@pik-potsdam.de)

P. Heimbach, Massachusetts Institute of Technology; EAPS, Room 54-1421; 77 Massachusetts Avenue; Cambridge, MA 02139. (heimbach@mit.edu)

(Received May 13, 1998; revised December 15, 1998; accepted January 19, 1999.)